

Citation for published version:
Nicassio, F, Scarselli, G, Pinto, F, Ciampa, F, Iervolino, O & Meo, M 2018, 'Low energy actuation technique of bistable composites for aircraft morphing', *Aerospace Science and Technology*, vol. 75, pp. 35-46. https://doi.org/10.1016/j.ast.2017.12.040

10.1016/j.ast.2017.12.040

Publication date: 2018

Document Version Peer reviewed version

Link to publication

Publisher Rights CC BY-NC-ND

University of Bath

Alternative formats

If you require this document in an alternative format, please contact: openaccess@bath.ac.uk

General rights

Copyright and moral rights for the publications made accessible in the public portal are retained by the authors and/or other copyright owners and it is a condition of accessing publications that users recognise and abide by the legal requirements associated with these rights.

If you believe that this document breaches copyright please contact us providing details, and we will remove access to the work immediately and investigate your claim.

Download date: 07, Mar. 2023

Low energy actuation technique of bistable composites for aircraft morphing

F. Nicassio * G. Scarselli * F. Pinto + F. Ciampa + O. Iervolino + M. Meo +

Universitá del Salento*, University of Bath† m.meo@bath.ac.uk

Abstract

Use of morphing structures for lightweight and energy-efficient aircraft mobile surfaces have been investigated for several years. This paper presents a novel lightweight, passive and low-energy morphing surface concept based on the "lever effect" of bistable composite plates that can be integrated in aircraft moving surfaces. The bistable composite plate mechanism is conceived to snap between two stable state producing an upward or downward movement of the aero mobile surfaces. By using appropriate boundary conditions, it was demonstrated that the magnitude of the activation force on the bistable composite was tailored to match the differential pressure on the aircraft's airfoil. As a consequence, the bistable laminate can be used as a passive morphing surface. Both numerical simulations and experimental testing were used to demonstrate this concept on a NACA 2412 airfoil structure. The results showed that, by choosing a proper configuration of constraints, lay-up and aspect ratio of the bistable plate, it was possible to tailor and activate the snap-through mechanism in a passive manner. We prove that this mechanism enables morphing of aerodynamics surfaces without sophisticated control when compared to an active morphing concept. The proposed passive morphing would provide a new avenue in aircraft mobile surfaces design that makes future morphing surfaces lighter and more energy efficient.

Keywords: Bistable Composites, Morphing Structures, Passive Structures, Smart Materials.

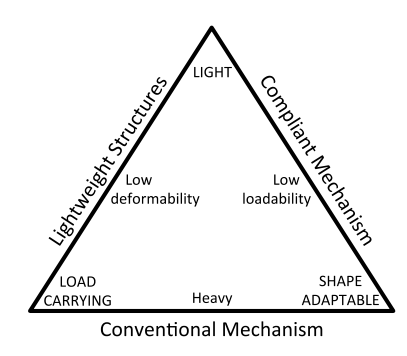
1. Introduction

The ability to adapt the aerodynamic shape of an aircraft to the environment in which it operates represents a key factor in the development of a new generation of air vehicles and it has been the focus of several researches during the last decades [1]. This conformal change (morphing ability) can enhance the aircraft capabilities in terms of maneuverability, fuel efficiency, and ability to perform dissimilar tasks in an optimal manner.

The current standard approach to modify the geometry of an aeronautical structure is to use conventional mechanisms such as hinged flaps on airfoils that can place limitations on the performance and lower the efficiency [2]. In the early years of aircraft design, rigid-body mechanisms were not the standard approach. Wright brothers [3] used structural flexibility, such as the wing-warping solution to control the roll and yaw of their vehicle, because a rigid body solution would be significantly heavier.

However, as aircrafts became more and more advanced, these flexible solutions were not efficient since stronger structural parts were required in order to lift the fuselage off the ground. As a consequence,

movable flaps, ailerons and slats made of stiffer materials such as aluminum and steel, were introduced into the wing structure with the disadvantage of weight increase and lower overall efficiency generated by the drag increase.



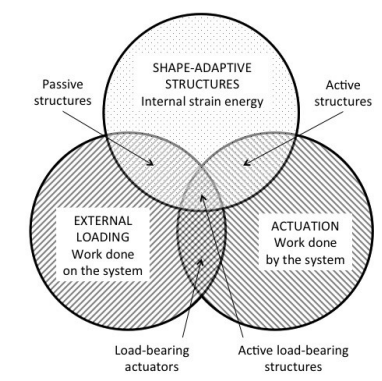


Figure 1: The structural requirements for lightweight shape adaptation.

Figure 2: The interaction between an adaptive structure, its external loading and actuation for a generic morphing system.

Hence, it is clear that in order to overcome the drawbacks of traditional moving parts, a shape adaptive structure concepts should satisfy the following three requirements, i.e. compliance, load carrying capability and low mass. These requirements can be represented by the triangle for lightweight shape adaptation shown in Figure 1. The interaction between these important design variables can be considered as a balance of energy between the work done on the system (external loading), the work done by the system (actuation) and the internal strain energy of the adaptive structure.

Aircraft moving surface can be activated in an active or passive manner. Clearly a passive surface, while satisfying all the structural and performance requirements, would be preferable due to lack of an actuation system, costs and potentially weight saving. As it is possible to see from Figure 2, by matching the internal strain energy of a shape-adaptive surface with the loads applied to the structure (work done on the system), it is possible to develop a system which can be defined as *passive*. Such a system will be able to respond autonomously by activating the morphing mechanism when an external force overcomes a specific threshold (which is defined by the constraints and the structural characteristics of the specific part) without the use of actuators or other mechanical devices.

In recent year the use of multistable composites has been investigated as a mean to morph aircraft surfaces. Multi-stable composites are structures capable of varying their shape when a force is applied in an appropriate location. Based on these premises, multi-stable composites constitute an interesting candidate for the development of such passive morphing structures. These structures exhibit multiple statically stable shapes, which can be designed to show different directional stiffness as described by many authors (e.g. Barbarino et al. [4] and Arrieta et al. [5], [6]). Changes between states occur due to externally forced deflections triggering a phenomenon known as *snap-through mechanism* which may involve large deflections of the laminate depending on the designed shapes and boundary conditions. In addition, considering the high level of customizability which is intrinsic of all composite systems, the mechanical properties can be easily tuned to match the external loading distributions with the force required to activate the snap-through mechanism. As a result, the energy provided by the external load can be effectively used to trigger a change to a different shape configuration, making these materials suitable components for shape morphing.

Daynes et al. [7] considered the composite bistable airfoil as a coupled structure-mechanism system. The actuator system and the aerodynamic loads were also coupled to the structure. The analysis performed in

this work was divided into two steps: an aeroelastic analysis which couples the adaptive structure with variable aerodynamic loads and an analytical model formulated to simulate the interaction between the structural and aerodynamic stiffnesses. Inviscid calculations of the aerodynamic pressure distributions around the airfoil were then carried out in order to assess the load carrying capability of the structure. The airfoil flap could remain in one of two stable geometries and both states were able to withstand the aerodynamic loading without any additional holding forces or locking mechanisms. However, in order to activate the transition between the two stable geometries, an external actuator is required. Based on the results obtained in their previous work, the same authors presented in [8] the design and wind tunnel test results of a full-scale helicopter rotor blade section with an electromechanically actuated bistable trailing edge flap. In the first stable state the flap follows the profile of the standard rotor blade section, while in its second stable state it deflects the trailing edge downwards. The flap system was designed to change between these two positions when the helicopter moves between hover and forward flight conditions. The bistability of the flap system allowed the rotor blade to keep the shape without the application of continuous loads, however it still required an electromechanical actuator to activate the snap-through mechanism between the two stable states. In this context, Bilgen et al. [9] investigated the reversible dynamic snap-through mechanism of a bistable composite plate with a clamped edge actuated by a surface mounted piezoelectric material. Following a numerical and experimental approach they concluded that by using micro fibre composite (MFC) transducers it was possible to actuate a bistable plate system able to carry out a wide range of aerodynamic loads.

The present work is focused on demonstrating a novel passive morphing concept. The main goal was to overcome the current limitations of bistable based morphing structures, by focusing on the development of a passive morphing system that does not require transducers or servo-actuators to activate the snap-through mechanism and can be integrated in flap structures or other moving parts of an aircraft. This morphing system comprises a bistable composite plate, whose mechanical characteristics and boundary conditions can be tailored to function as a traditional flap by exploiting specific values of the differential pressure between lower and upper camber of the airfoil to activate the snap through mechanism.

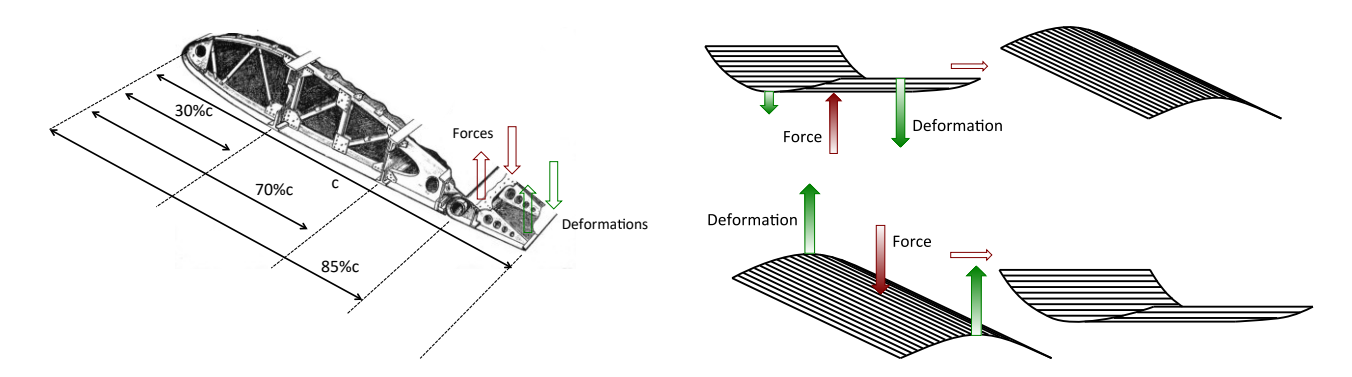


Figure 3: Forces on airfoil and on the bistable plate.

In order to properly tune the activation force of the bistable plate, a series of constraints were introduced in

the flap configuration so that by choosing the correct actuation load location it was possible to induce the snap-through movement only when specific values of the external pressure distribution are reached. Moreover, since the activation force needed to modify the bistable shape downward/upward is directed in a reverse way with respect to the differential pressure distribution (see Figure 3), the same constraints can be used in a "lever configuration" to invert the direction of the shape-change according to the system requirements. Numerical studies were conducted to analyse the pressure distribution on the airfoil in order to choose the optimal actuation load location. A coupled thermal structural FE model was then implemented in order to compare post-cure deformation shapes and actuated deformations of the laminate to tailor the mechanical characteristic of the composite part with the system requirements. The numerical-analytical models were validated via an experimental campaign by constraining the bistable plate in a specifically designed multifunctional frame. The main finding of this work is that a passive flap with a bistable plate that can be activated with a proper configuration of constraints and the order of magnitude of the activation force for the snap-though is the same of differential pressure on the airfoil.

The main finding of this research work is the design of a specific configuration of constraints for the bistable laminate that allow minimising the activation force to match specific values of the differential pressure on the airfoil.

In this way the bistable composite can be integrated in a low energy passive flap able to autonomously respond to pressure variations by decreasing the lift when a maximum altitude is reached and vice versa.

2. Pressure distribution on a typical aircraft mobile surface

In order to quantify the level of pressure distribution (i.e. the external load) needed to move an aircraft mobile surface, a typical NACA 2412 airfoil (widely used in small aircrafts and gliders) was considered in this study. This will allow to drive the design of the bistable morphing laminate, force needed for the snapthrough mechanism and the associated "lever effect". The chosen mobile surface is the flap, a device used to alter the airfoil lift characteristics and mounted on the trailing edges of the wings. The lift, L, is an external load and depends on environmental and structural variables (air density ρ , air speed V, wings surface S and lift coefficient C_L) according to the following formula [10]:

$$\mathcal{L} = \frac{1}{2} \rho V^2 S C_L \tag{1}$$

When the passive structure is activated, the geometry changes and modifies lift and pressure distributions. At fixed altitude and speed, the lift changes when the wing surface or the lift coefficient change and the next equation shows the relation between lift and pressure coefficients C_L and C_p on the lower $(C_{p,lower})$ and upper $(C_{p,upper})$ airfoil surface :

$$C_L = \int_0^1 \left(C_{p,lower} - C_{p,upper} \right) d(x/c) \tag{2}$$

where x is the coordinate along the chord c. C_p represents the local pressure on the airfoil p(x), related to the free stream air pressure p_{∞} , scaled down by the dynamic pressure $\binom{1}{2}p_{\infty}V_{\infty}^2$ with free stream air speed V_{∞} and density p_{∞} :

$$C_p(x) = \frac{p(x) - p_{\infty}}{1/2 \rho_{\infty} V_{\infty}^2} \approx 1 - \left(\frac{V}{V_{\infty}}\right)^2$$
(3)

In order to analyse the pressure distribution on the airfoil with and without the flap extended during a transition from the cruise flight level to a lower altitude, XFOIL software was used. This is an interactive program widely used for the design and analysis of subsonic isolated airfoils, and it was developed by MIT in the 1980s [11]. With NACA command, XFOIL gives the main characteristics of the airfoil and due to the low speed considered in this work, inviscid analyses were run. With an angle of attack of 5°, the pressure distribution on NACA 2412 is plotted in Figure 4. To decrease lift, a negative flap deflection occurs and so the pressure distribution on NACA 2412 with a deflection of -5° of flap (hinge on 85% of chord, in Figure 3) is plotted in Figure 5.

The upper surface and relative C_p distribution are plotted with continuous lines, whilst the lower surface and relative C_p are show in dashed lines. Negative/positive values of C_p indicate a local smaller/higher pressure than asymptotic one. The hinge position was taken as a reference point.

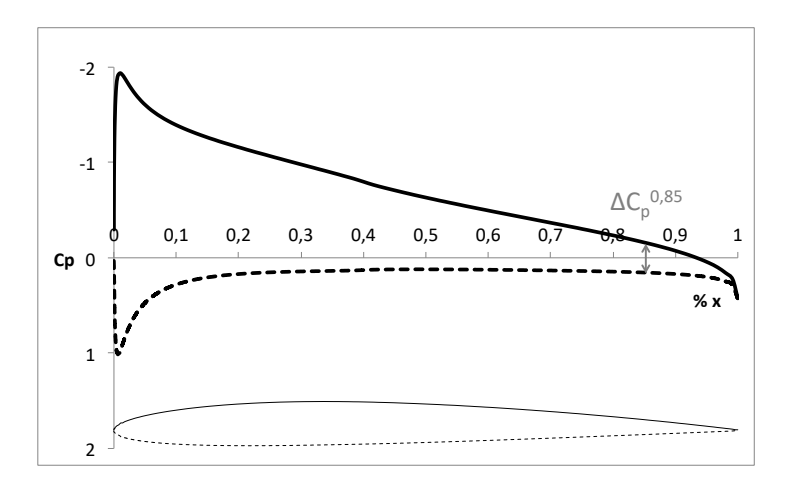


Figure 4: NACA 2412 Cp distribution.

In the case of 0° flap, $\Delta C_p^{0.85}$ = -0.3295 means that a net force is directed from a lower surface to an upper one. This external load can activate the flap in order to move the mobile surface and change the pressure and lift distributions.

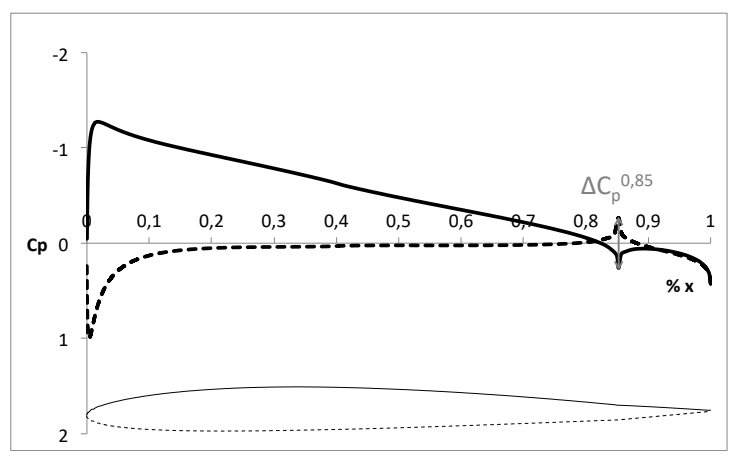


Figure 5: NACA 2412 with -5° flap Cp distribution.

With an upwards external load, the flap has a negative deflection and the C_p distribution shown in Figure 5 has a particular behaviour at the reference point: with $\Delta C_p^{0.85}$ = 0.4038, a net force is directed from an upper surface to a lower one. Now, a downward load can reactivate the mobile surface in order to return to the previous configuration.

The results obtained in Figures 4 and 5 determine the requirements for designing a bistable composite as a passive morphing surface integrated in an aircraft wing flap, so that the aerodynamic pressure acting on the NACA 2412 airfoil will match the forces needed to activate the snap-through mechanism. Moreover, as the differential pressure distribution is directed in a reverse way with respect to the bistable active force's direction (see Figure 3), specific boundary conditions will be adopted (via the "lever configuration") to to activate the snap-through in the required direction. This will be the topic of the following section.

3. The lever effect

As mentioned in the previous section, to activate the flap from 0° to -5° the external load is directed upward. In a first approximation, the bistable plate can be idealised as a beam. In order to allow the snap-through movement from one stable state to another, the following concept was developed as illustrated in Figure 6.

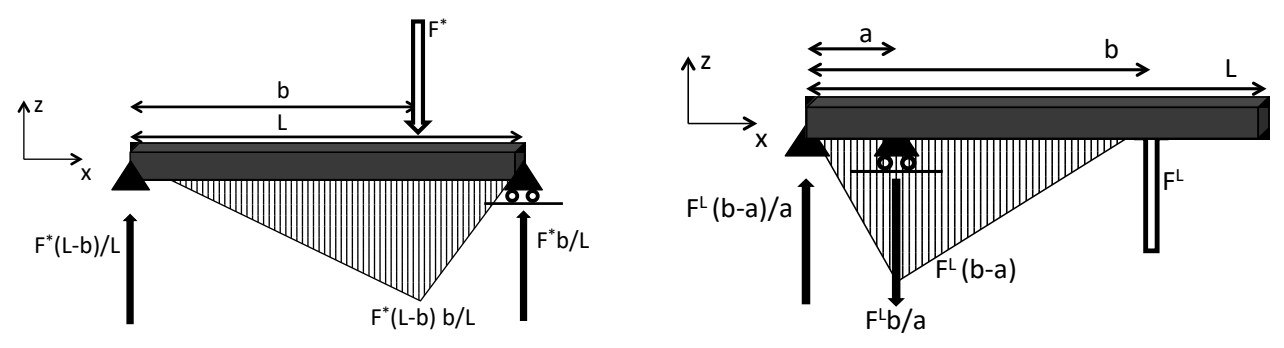


Figure 6: Beam moment diagram with simple supports (left) and with lever (right).

If the beam is simply supported at the ends (standard configuration) and loaded by a point load along the span in b, the constraint forces and the bending moment follow the scheme represented in Figure 6 (left). A downward force is necessary to activate the snap-through in opposition to the external load on the airfoil. In order to generate an upward activation force, a support (septum) is introduced at a coordinate a between the point load and the support at the other end (lever). As shown in Figure 6 (right), the bending moment diagrams follow the same trend, with opposite activation forces. The focus is that the transition is activated by external forces as soon as the local bending moment reaches a proper threshold.

The local bending moment $M^*(x)$ can be evaluated for the structural simply supported scheme as follows:

$$M^*(x) = \frac{F^*(L-b)}{L} x \underset{b=BL}{\xrightarrow{x=XL}} M^*(X) = F^*L(1-B)X$$
(4)

where b = BL, x = XL and B and X are non-dimensional parameters between 0 and 1. As $M^*(X)$ reaches a threshold, the transition of the bistable plate from a configuration the other one occurs.

In the lever case, the bending moment reaches the highest value at the coordinate a:

$$M^{L}(a) = F^{L}(b-a) \underset{b=BL}{\Longrightarrow} M^{L}(A) = F^{L}L(B-A)$$
(5)

Under the assumption that the threshold bending moment M^* necessary to snap from one stable configuration to the other remains the same between the two analysed configurations, it is possible to use the equations (4) and (5) to evaluate the effects of the lever on the activation mechanism. The basic consequence of the lever is a different pattern along the beam length. For the activation, it must be verified that

$$M^L \ge M^* \tag{6}$$

and this means (assuming that $F^L=F^*$ and X=A)

$$F^{L}L(B-A) \ge F^{*}L(1-B)A \Longrightarrow_{F^{*}=F^{L}} A \le \frac{B}{2-B} = A^{*}$$
 (7)

In Figure 7 (with B=0.5 and consequently $A^*=0.333$) it is clear that, for $A \le A^*$, the bistable can be activated with the same value (but opposite direction) of F^L and F^* , since the threshold bending moment M^* is exceeded. From the same image, it is also clear that for A=0.4 there is not activation since the moment M^L is smaller than M^* .

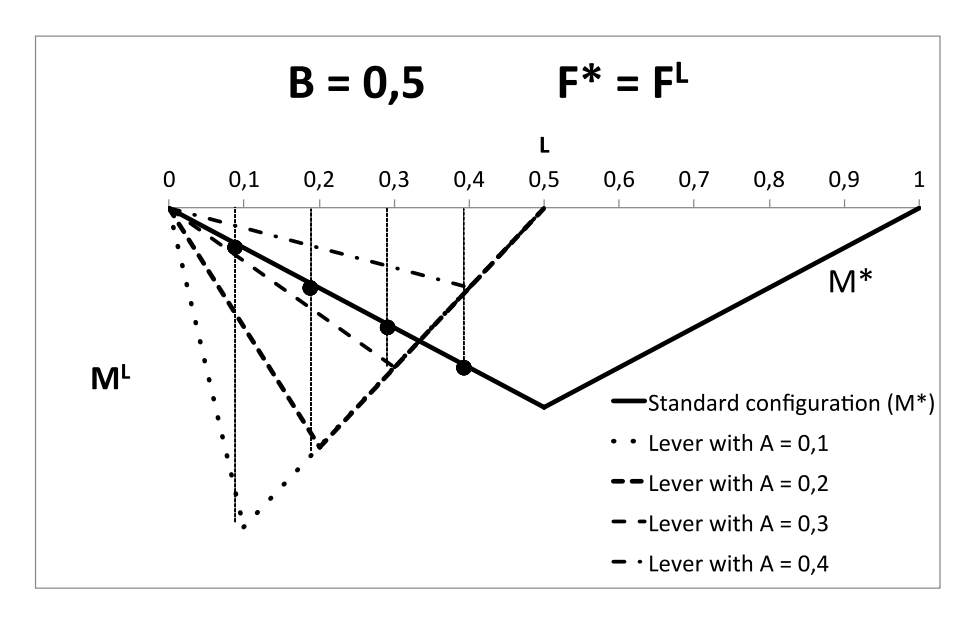


Figure 7: Bending moment for standard configuration (without lever) and for lever configuration.

Analysing the requirements in terms of activation force it is also possible to observe that when the lever configuration is applied to the bistable plate, the snap through mechanism is activated with a smaller force than the one needed for a standard configuration, as shown in the equation below:

$$\frac{F^L}{F^*} = \frac{A(1-B)}{(B-A)} \tag{8}$$

Since the previous threshold A^* was calculated with the hypothesis of $F^L = F^*$, it is clear that, removing this hypothesis, if $A = A^*/2$, than $F^L/F^* = 1/2$, if $A = A^*/3$, than $F^L/F^* = 1/3$ and so on.

In conclusion by applying specific constrains into the lever configuration it is possible to have two distinct benefits: the septum will allow to activate the bistable with a force that is opposite to the one used in the standard configuration and, by choosing properly A and B, it is possible to reduce the activation force F^L in respect to F^R so that it is possible to tune it with the pressures evaluated in section 2.

4. Snap-through process: activation forces and deformations

A thermal-mechanical numerical Finite Element (FE) model was developed to design the bistable composite as a passive morphing surface by matching the aerodynamic pressure acting on the NACA 2412 airfoil (see Section 2) with the forces needed to activate the snap-through mechanism. The entire analysis was split up

in two load cases: the thermal simulation to induce the curved shape and the transient simulation of the snap-through deformation. The commercial software ANSYS® 15.0 was used [12]. The bistable rectangular plate (240mm × 120mm) is made up by stacking 4 laminae following a [0₂/90₂] sequence. The material used was a carbon prepreg T800/M21 (see [13] for the mechanical properties) manufactured by Hexcel. For the first load case (cooling down), the goal was to simulate the deformed shape due to the thermal residual stresses. The temperature profile, applied to the mesh nodes, was a linear ramp from 150 °C to 15 °C. The panel was modeled using 480 shell element [14]. Convergence studies on the mesh size were carried out in order to determine acceptable accuracy of the model. The option "Large Deflection" was employed in each step because of large deformation for small load increments of the plate during the process (geometric nonlinearity). Convergence also depends on the boundary conditions: two simple supports on the middle nodes on the short sides of the rectangular plate and two rotational constraints on the same nodes along direction "y" (see Figure 8 for directions x, y and z) were applied. Various load cases were analysed to study the bistable behaviour in various boundary conditions (variable positions of the septum) and activation force positions as shown in Figure 8 (each triangle represents the constraint to the displacement in that direction).

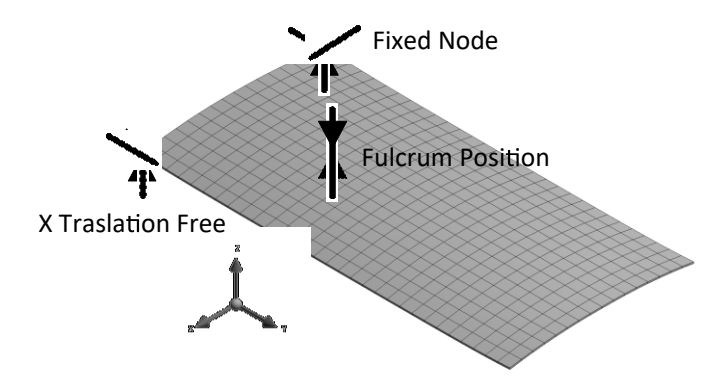


Figure 8: Bistable panel boundary conditions.

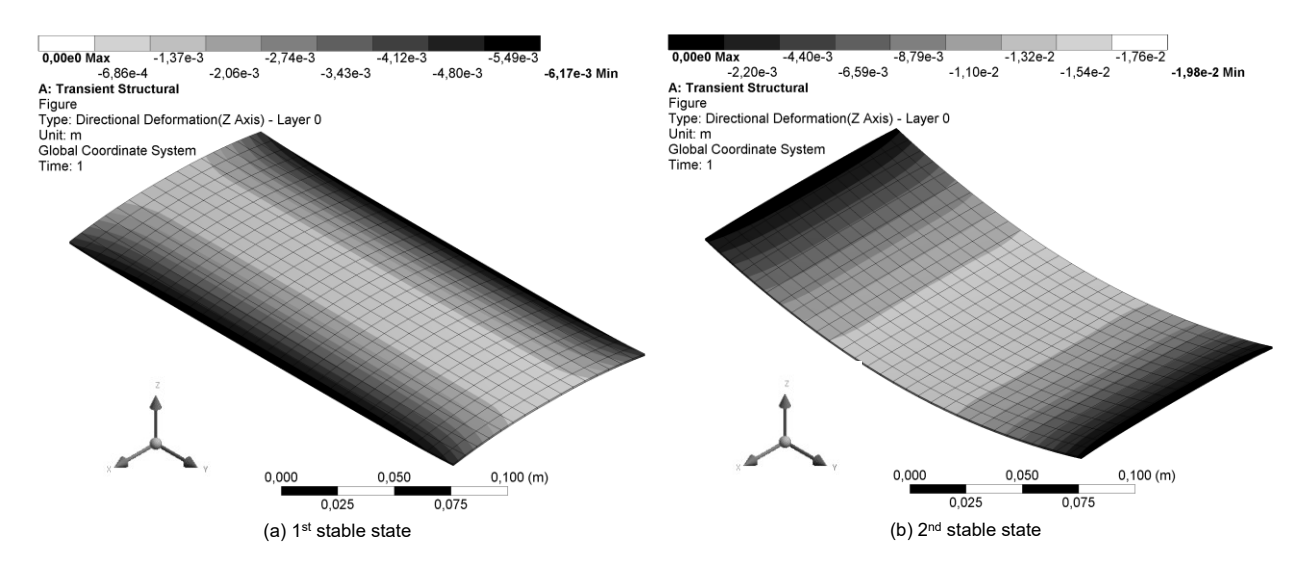


Figure 9: Bistable panel model and the two stable state shapes.

Typical bistable deformations are shown in Figure 9. The contours illustrate that each side, for both the stable states, has a curvature as stated by Gauss in his "Theorema Egregium" [15]. The theorem enunciates that the Gaussian curvature of a surface (the product of the principal curvatures at a point) is an intrinsic invariant. In the bistable composite plate under investigation, the Gaussian curvature is strictly negative in both stable shapes since the two principal curvatures are of opposite sign. The unstable state, at the transition between two stable states, is a saddle, which is a peculiar geometry with negative Gaussian curvature [16].

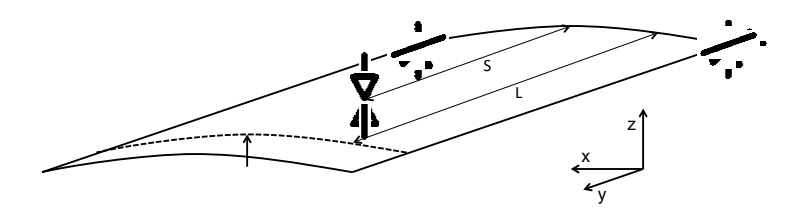


Figure 10: S (septum position) and L (load position).

In order to understand the meaning of the symbols "S" and "L" used throughout the text, Figure 10 can be used as a reference: "S" indicates the distance in mm of the septum position whereas "L" indicates the distance in mm of the load position. Some configurations of boundary conditions and loads for transition from the first stable state (ST1) to the second stable state (ST2) were not investigated and not reported because they were not suitable for the adopted experimental set-up.

S [mm]	L [mm]	F [N] from ST1 to ST2	F [N] from ST2 to ST1
40	200	2.08	-1.15
40	240	1.85	-0.96
	160	8.30	-3.20
80	200	5.80	-2.20
	240	4.50	-1.77
	160	23.50	-9.00
120	200	12.10	-4.70
	240	9.30	-3.40
160	200	27.90	-9.40
160	240	15.40	-4.40
200	240	23.30	-7.50

Table 1: Activation forces for each boundary condition.

S	Snan Through		Ex	:	Εγ	Uz
[mm]	Snap-Through	TOP	BOTTOM	TOP	BOTTOM	[mm]
40	ST1->ST2	- 4,21e-04	1,80e-04	- 4,62e-03	- 1,02e-03	77.02
40	ST2->ST1	8,43e-04	- 1,21e-03	1,33e-03	1,05e-03	77,02
80	ST1->ST2	- 4,21e-04	1,80e-04	- 4,33e-03	- 7,37e-04	55,36
80	ST2->ST1	8,43e-04	- 1,21e-03	1,03e-03	7,67e-04	33,30
120	ST1->ST2	- 4,21e-04	1,80e-04	- 4,17e-03	- 5,92e-04	42.36
120	ST2->ST1	8,43e-04	- 1,21e-03	8,82e-04	6,22e-04	42,30
160	ST1->ST2	- 4,21e-04	1,80e-04	- 4,03e-03	- 4,50e-04	28,34
100	ST2->ST1	8,43e-04	- 1,21e-03	7,35e-04	4,80e-04	20,34
200	ST1->ST2	- 4,21e-04	1,80e-04	- 3,89e-03	- 3,27e-04	1467
200	ST2->ST1	8,43e-04	- 1,21e-03	6,03e-04	3,57e-04	14,67

Table 2: Deformations and displacement for each boundary condition.

The numerical results provided by FE models allow to define: (i) the activation forces for the snap-through in Table 1 that will be compared with the experimental results and with the external load on the airfoil in the following paragraphs, (ii) the maximum deformations (for the top and the bottom of the plate) that define the geometry of the two stable states and (iii) the displacements (Table 2) for different septum positions. As illustrated in Table 3, the deformations in the x-direction ε_x have constant values and this result confirms that the bistable plate can be idealised as a one-dimensional element, whilst the deformation in y-direction ε_y and the z-displacement u_z have an almost linear trend shifting the septum, as illustrated in Figure 11. These values of displacements should be compared with the actual displacement of the conventional flap to evaluate the feasibility of the employment of bistable plate as a mobile surface. If a flap long 15% of the chord c is

considered on an airfoil of 2000 mm of chord length, a deflection of -5° will result in a vertical displacement of 26 mm. From Figure 11 (left), it can be noticed that this value is comparable with the vertical displacements of the bistable plate that are reported for different septum positions.

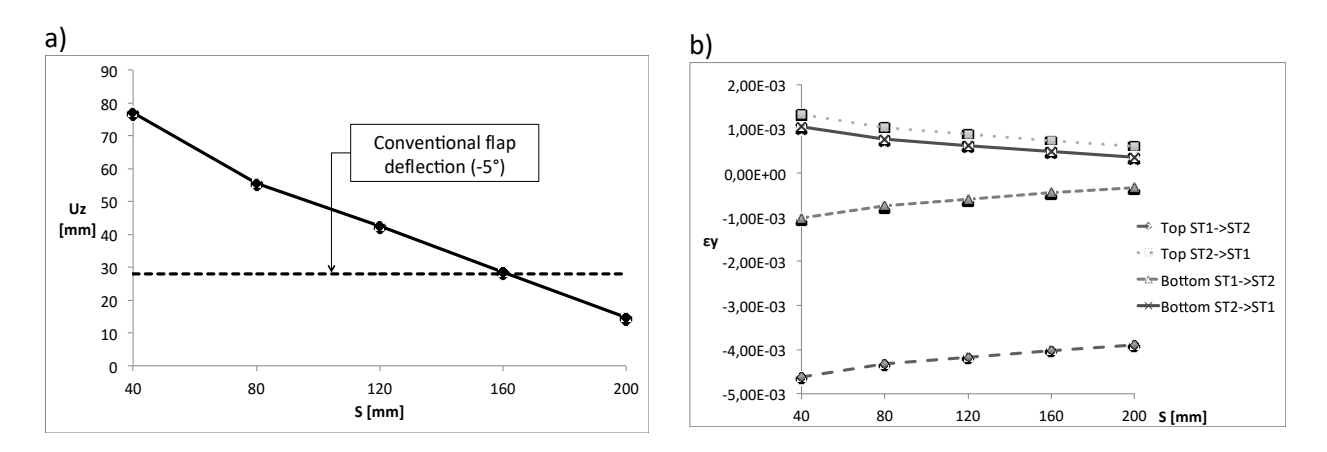


Figure 11: Displacements (a) and deformations (b) with different septum positions.

5. Experimental tests

The numerical simulation results showed that via exploiting the lever configuration a significantly lower activation force is required to activate the snap-through mechanism in comparison with the traditional configuration. In order to find experimentally the forces needed to activate this mechanism, a number of four-layer asymmetric carbon fibre reinforced plastic (CFRP) laminates were fabricated. The nominal thickness of the initial carbon pre-preg sheet was 0.125 mm, and the total laminate thickness was 0.5 mm. Samples were cured in autoclave using two different curing cycles to study the relation between curing temperature and activation forces. The first sample was cured following the traditional cycle suggested by the producer, setting the temperature at 180°C with a rate of 5 °C/min, while a second batch was prepared at 150°C (with a rate of 5 °C/min) with the overall curing cycle of 3 hours. In order to increase the generated stresses and obtain a higher level of curvature in the samples, both laminates were removed from the autoclave immediately after the curing reaction and rapidly cooled down in open air instead of following the cool rate of 2-5 °C/min suggested by the manufacturer.

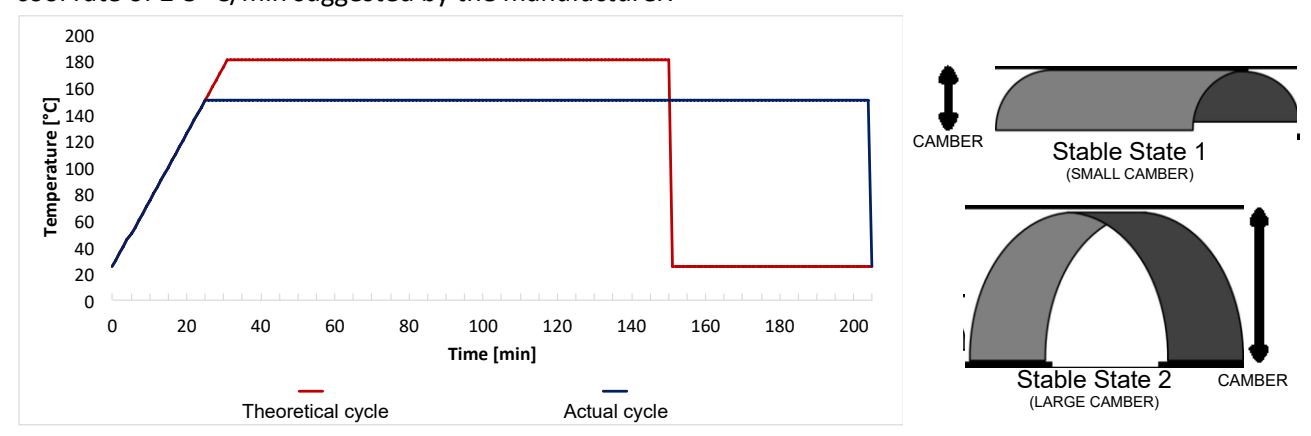


Figure 12: Curing profiles and stable states.

Both cure cycles are represented in Figure 12 below and the maximum camber measure in the two stable reported in Table 3.

	Sample 1 (Curing T	emperature 150 °C)	Sample 2 (Curing Temperature 180 °		
	Stable state 1 Stable state 2		Stable state 1	Stable state 2	
Maximum Camber	6.28 mm	18.22 mm	7.60 mm	19.50 mm	

Table 3: Maximum camber.

Upon cooling to room-temperature, the manufactured laminates were observed to have two stable states of curvature, as reported in Figure 12. The curvatures are due to a mismatch in the thermal expansion behaviour of the layers within the laminate. These particular characteristics are common in asymmetric laminates when subjected to a thermal field that varies with time [17], [18]. It is important to underline that although the asymmetric thermal expansion is the main cause for the stress generation, there are others factors that must be taken into account in order to obtain the desired geometry of the final part. Indeed, as evidenced by Hamamoto et al. the ply thickness is of particular importance, observing that also a variation of 1% can have a significant effect on the final configuration of the laminate and prevent the onset of the bistability [19].

Other studies noticed that also the type of pre-preg and the amount of humidity during the manufacturing process have to be taken into account and can affect the final shape of the sample [20]. Based on these premises, it is possible to conclude that the only asymmetric nature of the stacking sequence does not ensure bistability. Indeed, another key factor is the edge lengths to thickness ratio, as higher curvature can be achieved when thinner laminates of the same material are used. Keeping constant the other parameters, and considering a CFRP laminate with this lamination sequence, it was found that for small laminates the saddle shape is the only stable configuration. This shape remains stable until the length of the samples does not reach a specific threshold. Above this critical value, the saddle shape becomes unstable, and two stable cylindrical configurations occur. The snap-through mechanism between the two stable shapes is activated with a small energy input. The two cylindrical shapes present inverse sign of the curvature, offering a large deflection with relatively small and removable energy. These two factors (large achievable displacements and low energy requirements) are the main reasons for the increasing interest about bistable composite laminates, in particular for applications such as morphing structures [21].

The actuation force required to activate the snap-through mechanism is highly dependent on the degree of the laminate curvature, the material properties and the curing cycle. Indeed, for the sample cured at 180 °C, the force required to shift between the two different stable configurations is higher respect to the laminate cured at 150 °C. Moreover, as stable state 2 is characterised by a maximum camber higher than stable state 1 (see Figure 12), the force required to activate the snap-through mechanism results lower for the 1-2 transition than the one required for the inverse movement 2-1. In order to obtain a higher effectiveness of the system, the sample cured at lower temperature was chosen for the experimental setup. Table 4 reports the comparison between the numerical (see Section 4) and experimental results. An error less than 9% was found for all the stable configurations.

	Simulated Camber [m]	Measured Camber [m]	Error [%]
1 st stable shape	6.17 x 10 ⁻³	6.28 x 10 ⁻³	1.75
2 nd stable shape	19.81 x 10 ⁻³	18.22 x 10 ⁻³	8.73

Table 4: Simulated and measured cambers.

The force required to activate the snap-through transition between the two different states of the bistable was evaluate by developing a specific test rig as represented in Figure 13.

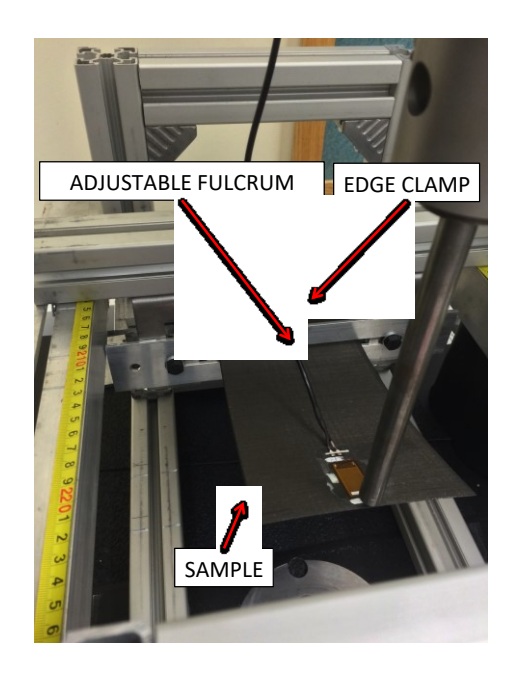
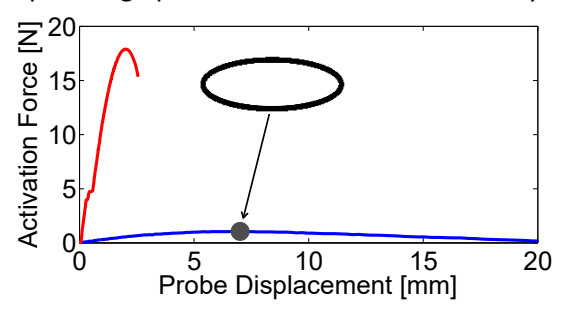
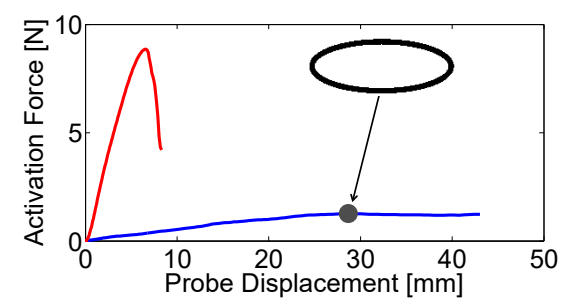


Figure 13: Snap-through force evaluation test setup.

Since the sample must be constrained in several configurations in order to optimise the snap-through activation force, a particular attention was given to the support required to hold the sample during the test that was specifically designed and manufactured. As it is possible to see from Figure 13, the holder is formed by a frame made with t-slotted aluminium profiles equipped with two moving parts on rails so that it is possible to adjust each side of the support structure and fix one edge of the sample with a clamp, while a septum can be regulated along the entire length of the aluminium profile in order to move a support constrain. As a result, the final configuration can be described as a hyperstatic simply supported cantilever beam. The entire system was regulated along the out of plane direction by lifting both the supports (clamp and septum) so that can easily fit below different models of Instron Tensile machines. A support laser vibrometer was mounted on the opposite side of the frame to measure the out-of-plane displacement and evaluate the velocity, acceleration and damping factor of the sample.

The actual activation forces experimentally obtained in several configurations of constraints are here analysed and discussed. The Instron®machine was set in order to operate in "steady-state" mode due to the low crosshead speed (maximum 50mm/min). Because the Instron®machine measures the plate reaction force, the load curves in Figure 14 show a maximum value after an almost linear behaviour; the reaction force then decreases immediately after the maximum value due to a redistribution of internal stresses during the snap-through phenomenon. For sake of clarity only the two extreme load curves are reported.





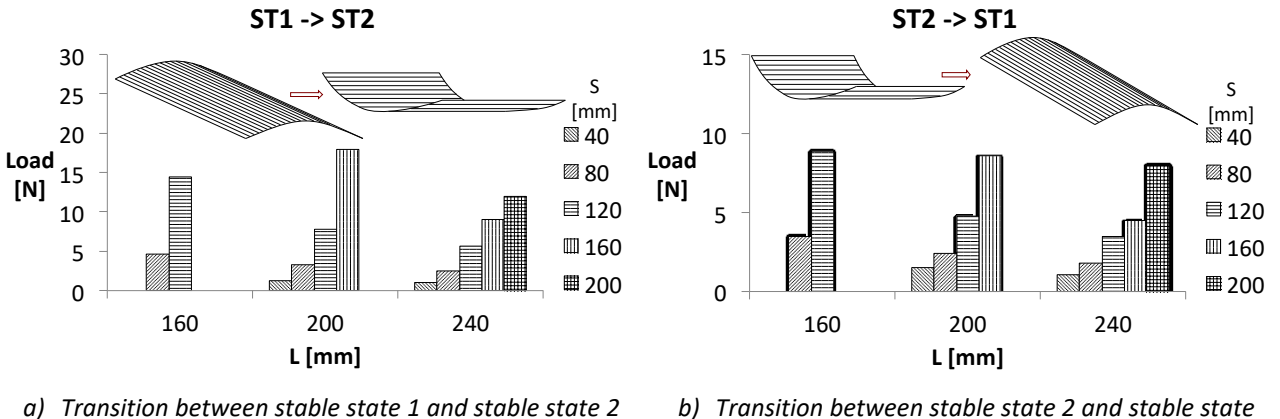
Transition between stable state 1 and stable state 2

Transition between stable state 2 and stable state 1

Figure 14: Activation forces with variable position of load (L) and septum (S).

Figure 14 reports the experimental results associated to the activation forces acquired for different configurations of load and constraints, which result in different values of *S* and *L*. In addition it can be noticed

that the force needed for activating the transition between state 1 and state 2 is bigger than the one needed for the opposite transition (from state 2 to state 1). This difference vanishes when the lever is exploited since the activation forces become small and of similar magnitude. For both the transitions between the two stable states, a minimum activation force can be determined (see Figure 14), corresponding to a specific value of S and L.



- b) Transition between stable state 2 and stable state

Figure 15: Activation forces with variable septum position (S) for different points of load application (L).

Figure 15 shows the maximum value of load for each combination of S and L, which corresponds to the activation force. This figure highlights the following important result: the actual activation force responsible for the transition between the two stable states decreases by shifting the application point towards the free edge (i.e., increasing L) and the septum position towards the constrained edge (i.e., decreasing S). The optimal configuration which generates the lowest combination of snap-through forces is the one with septum position S = 40 mm and load position L = 240 mm. Hence, by using the "lever effect", the magnitude of the activation force on the bistable composite can be reduced to match the differential pressure on the aircraft's airfoil an autonomously activate the snap-through mechanism.

6. Experimental/numerical correlation

The bistable composite FE model simulates the plate behaviour with some differences due to boundary conditions and applied load. In the numerical simulations perfect simple and cylindrical supports are modelled and constraint's friction and flaws are neglected. During each experiment, the Instron crosshead applied the force on different plate points because of composite large deformations, but in the ANSYS model the activation force was acting always on the same node during the entire analysis. Furthermore, at the transition between the two stable states, there are relevant inertial effects that are not sensed by the Instron probe, since the plate accelerates and loses contact with the load cell. These inertial terms must be added to the loads read by the Instron to make a comparison with the numerical activation loads. The discrepancy between the experimental configuration and the model causes the errors between the actual activation forces and the virtual ones represented in Table 5. When the crosshead did not lose contact with the sample, accelerations were not used and no inertial effects were considered. As it is possible to see from the results, in these cases there is a good agreement between the numerical and experimental activation forces. It is clear from the Table 5 that, taking into account the inertial effects, a reasonable agreement between the numerical model and the experiments can be achieved.

			Instron Load	Acceleration	Inertial Load	Tot Load	Ansys Load	Error
	[mm]		[N]	[m/s ²]	[N]	[N]	[N]	[%]
Support	40							
Load	200	ST1->ST2	1,30	25	0,92	2,22	2,08	6,17
	200	ST2->ST1	1,50			1,50	1,39	7,33
	240	ST1->ST2	1,08	17	0,62	1,70	1,85	8,61
	240	ST2->ST1	1,05			1,05	0,96	8,57
Support	80							
Load	160	ST1->ST2	4,60	142	4,17	8,77	8,30	5,31
	160	ST2->ST1	3,50			3,50	3,20	8,57
	200	ST1->ST2	3,30	81	2,38	5,68	5,80	2,18
	200	ST2->ST1	2,40			2,40	2,20	8,33
	240	ST1->ST2	2,50	63	1,85	4,35	4,50	3,50
	240	ST2->ST1	1,80			1,80	1,77	1,67
Support	120							
Load	160	ST1->ST2	14,50	434	9,55	24,05	23,50	2,28
	160	ST2->ST1	8,90			8,90	9,00	1,12
	200	ST1->ST2	7,80	184	4,05	11,85	12,10	2,13
	200	ST2->ST1	4,80			4,80	4,70	2,08
	240	ST1->ST2	5,70	177	3,89	9,59	9,30	3,06
	240	ST2->ST1	3,50			3,50	3,40	2,86
Support	160							
Load	200	ST1->ST2	18,00	690	10,12	28,12	27,90	0,78
	200	ST2->ST1	8,60			8,60	9,40	9,30
	240	ST1->ST2	9,00	406	5,95	14,95	15,40	2,98
	240	ST2->ST1	4,50			4,50	4,40	2,22
Support	200							
Load	240	ST1->ST2	12,00	1536	11,26	23,26	23,30	0,15
	240	ST2->ST1	8,00			8,00	7,50	6,25

Table 5: Experimental/numerical correlation.

With these virtual and real corrected models of the bistable plate, it is possible to calculate the aerodynamic forces to carry out a comparison with the activation forces of our examples. During a typical mission, the altitude variation induced by the motion of the flap, causes pressure and density changes. As an example, the goal is to modify the cruise altitude (h) from 3000 m to 200 m and vice versa, without using an active control: the pressure on the airfoil is the "passive control" to change the airfoil shape and, consequently, to target the goal. The International Standard Atmosphere (ISA with standard pressure p_{std} , density p_{std} and temperature T_{std}) can be used to simulate the air behavior:

$$p = 0.9877 \frac{h}{100} \, p_{std} \tag{9}$$

$$\rho = \rho_{std} * \left[1 - \left(\frac{6.5}{T_{std}} \right) \frac{h}{1000} \right]^{4.255}$$
 (10)

The assumption that the speed (55 m/s) remains constant during the entire maneuver is made. A conventional flap (hinge at 85% of the chord) is taken into account to obtain different lift coefficients and pressure distributions.

P.	Alt.	p∞	ρ∞	٧	Dyn. p	Delta	Cp @	985%c	i)	Δр
	[m]	[Pa]	[kg/m ³]	[m/s]	[kg/m/s ²]	[°]	Тор	Down	Тор	Down	[Pa]
1	3000	69898	0,9092	55	1375	0	0,1745	0,1549	69659	70111	452
2	3000	69898	0,9092	55	1375	-5	0,1389	-0,2649	70089	69534	-555
3	200	98848	1,2016	55	1817	-5	0,1389	-0,2649	99100	98366	-734
4	200	98848	1,2016	55	1817	0	0,1745	0,1549	98530	99129	599

Table 6: NACA 2412 characteristics.

In Error! Reference source not found. the numerical results obtained on the airfoil of the example are reported. They represent the aerodynamic properties of the flow around the airfoil in the different conditions of altitude, speed and flap deflections considered. The differential pressure reported in the last column will be the "tool" to activate the passive flap. The external forces to activate the bistable mobile surface can be obtained exploiting the different pressure between the top and the bottom of the airfoil. Two channels can be inserted on the wings surfaces as represented in Figure 16 in order to direct the air pressure to a specific load application location and activate the snap-through mechanism.

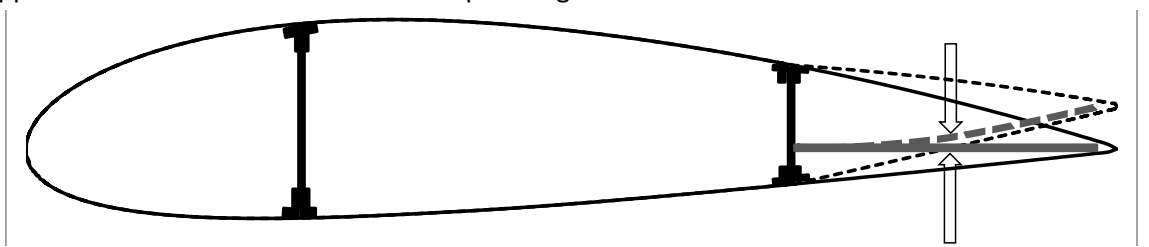


Figure 16: Sketch of the bistable flap

The rear spar is the clamp for the short edge of the bistable plate, the two gray triangles represent the intermediate septum and the two channels allow for the air to apply the force on the laminate when is exposed to the desired value of the differential pressure.

Simple calculations of the necessary holes radius can be made on the NACA 2412 airfoil considered in this study. The differential pressure must be compared with the experimental forces needed to activate the snapthrough. From Figure 11 (left), it can be noticed that the vertical displacement of a conventional flap is comparable with the vertical displacements of the bistable plate, assuming a septum position of 80 mm and a load location of 160 mm. Under these conditions, the needed forces F_{need} experimentally found are reported in Table 7, at the two altitudes taken into account in this example. The differential pressures are the ones previously calculated. Since

$$S_h = \frac{F_{need}}{\Delta p},\tag{11}$$

the condition imposed by the 3000 m altitude imposes that hole radius S_h is 78 mm (a smaller radius would not allow the activation).

F _{need} [N]	Δp [Pa]	S _h [cm ²]	R [mm]	F _{act} [N]
8,77	452	194	78	8,86

-3,50 -734 48 78	-14,39
-------------------------	--------

Table 7: Flap activation forces.

The magnitude of the activation force can be regulated to match the differential pressure on the aircraft's airfoil. Indeed, In Figure 17 the activation forces for the two snap-through motions are plotted for several boundary conditions. The dashed lines represent the actual forces on the airfoil, so each activation force value under these thresholds can be used to activate the bistable flap: the specific case (with septum position of 80 mm and load location of 160 mm) is suitable for the boundary conditions of the passive bistable flap.

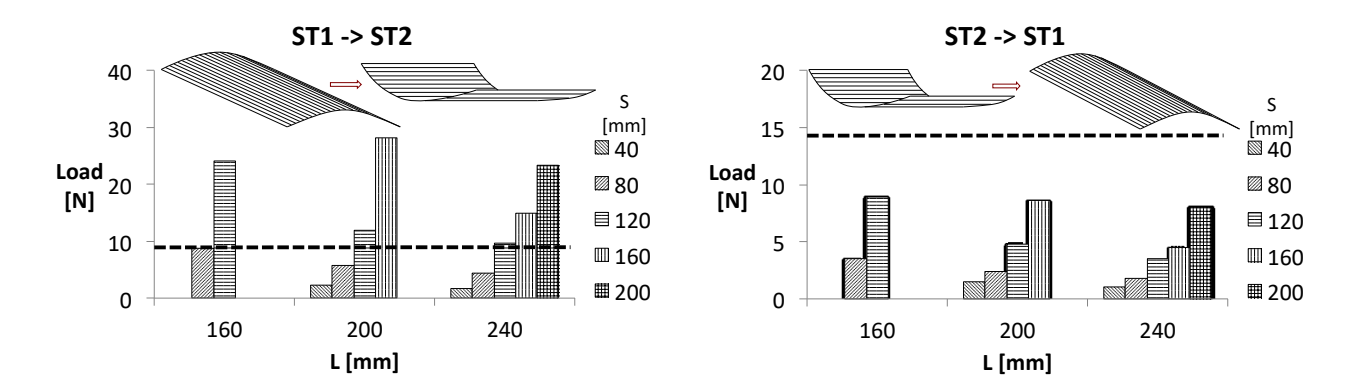
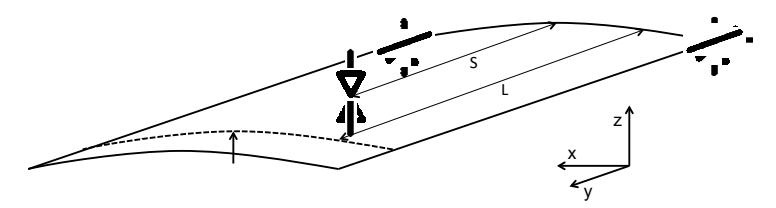


Figure 17: Activation forces vs available force (dotted line) due to differential pressure on the airfoil.



The results show that a significant reduction the activation force could be achieved with respect to a conventional bistable plates. In particular, it is demonstrated that the activation force needed for the snapthrough decreases by increasing L and decreasing S, i.e. the force activation location is closer to the free edge and the septum position is closer towards the constrained edge. The low actuation force would allow the bistable composite to be integrated in a low energy passive flap able to autonomously respond to pressure variations by decreasing the lift when a maximum altitude is reached and vice versa.

7. Conclusions

Morphing airfoil offers great potential for increasing the performance of future air vehicles. In this work, we presented a novel passive lightweight and low-energy morphing surface concept based on a bistable composite plate with specific constraints that can be integrated in an aircraft flap. This passive bistable morphing concept would allow a moving surface to change its angle of attack when a specific altitude and pressure is reached, without the need of electromechanical actuators. In particular, the bistable composite can be passively activated by the differential pressure load between the lower and upper camber of the airfoil. Hence, it can autonomously respond to pressure variations by decreasing the lift when a maximum altitude is reached and vice versa. By combining specific constraints into the "lever" configuration, two main considerations were drawn: (i) the bistable plate could be activated with a force that is opposite to the one acting on the wing as differential pressure and (ii) the magnitude of the activation force could be tuned to induce the snap-through mechanism. In this work, the concept was demonstrated on a NACA 2412 profile. This morphing concept could lead to lighter and more efficient aircraft morphing surfaces.

References

- [1] Barbarino, Silvestro, et al. "A review of morphing aircraft." Journal of Intelligent Material Systems and Structures 22.9 (2011): 823-877.
- [2] Dornier C., inventor; Dornier C., assignee. Control apparatus for aircraft. United States patent US 2315110 A. 1943 March 30.
- [3] Wright O., "How we invented the airplane: an illustrated history", Mineola, New York: Dover Publications, 1988.
- [4] Barbarino S., Pecora R., Lecce L., Concilio A., De Rosa L., "Airfoil Structural Morphing Based on S.M.A. Actuator Series: Numerical and Experimental Studies". *Journal of Intelligent Material Systems and Structures*, vol. 22, p. 987-1003, ISSN: 1045-389X, DOI: 10.1177/1045389X11416032
- [5] Arrieta A.F., Spelsberg-Korspeter G., Hagedorn P., S. A. Neild S. A., Wagg D. J., "Low order model for the dynamics of a bi-stable composite plate", *Journal of Intelligent Material Systems and Structures*, 2011, 22:2025–2043.
- [6] Arrieta A.F., Wagg D. J., Neild S. A., "Dynamic snap-through for morphing of bi-stable composite plates". *Journal of Intelligent Material Systems and Structures*, 2011, 22, 103-112.
- [7] S. Daynes S., Weaver P.M. and Potter K.D., "Aeroelastic Study of Bistable Composite Airfoils", *Journal of aircraft*, Vol. 46, No. 6, November–December 2009, University of Bristol, Bristol, England BS8 1TR, United Kingdom, DOI: 10.2514/1.44287.
- [8] Daynes S., Nall S.J., Weaver P.M., Potter K.D., Margaris P., Mellor P.H., "On a Bistable Flap for an Airfoil", 50th AIAA/ASME/ASCE/AHS/ASC Structures, Structural Dynamics and Materials Conference, Palm Springs, California, University of Bristol, Bristol, BS8 1TR, UK.
- [9] Bilgen O., Arrieta A.F., Friswell M. and Hagedorn P. "Dynamic control of a bistable wing under aerodynamic loading", *Smart Materials and Structures*, DOI:10.1088/0964-1726/22/2/025020.
- [10] Kuchemann, D. "The aerodynamic design of aircraft." Progress in aeronautical sciences, 1965, 6,271 (Pergamon, London) (1978).
- [11]Drela M. " XFOIL subsonic airfoil development system", http://web.mit.edu/drela/Public/web/xfoil/ (9/09/2014).
- [12]Inc. ANSYS. Workbench User's Guide Release 15.0, 2013.
- [13] Hexcel Corporation Carbon/Epoxy. Data Sheet Composite T800/M21 Unidirectional Prepreg, 2012.
- [14] Potter K.D., Daynes S., Diaconu C. G. and Weaver P. M., "Bistable prestressed symmetric laminates", *Composite Materials*, 44(9), 2010. DOI: 10.1177/0021998309351603.
- [15] Gauss K. F., General Investigations of Curved Surfaces of 1827 and 1825, The Princeton University Library, (1902).
- [16] Gray A., Abbena E., and Salamon S., Modern Differential Geometry of Curves and Surfaces with Mathematica, Chapman & Hall/CRC, (2006).
- [17] Hyer, M.W., "The room-temperature shapes of four-layer unsymmetric cross-ply laminates", *Journal of Composite Materials*, 1982. 16(4): p. 318-340.
- [18] Hyer, M.W., "Some observations on the cured shape of thin unsymmetric laminates", *Journal of Composite Materials*, 1981. 15(2): p. 175-194.
- [19] Akira, H. and Hye M., "Non-linear temperature-curvature relationships for unsymmetric graphite-epoxy laminates", *International Journal of Solids and Structures*, 1987. 23(7): p. 919-935.
- [20]Cox, S., et al., "Stress Free Temperature Testing and Residual Stress Calculations on Out-of-Autoclave Composites". 2012.
- [21]Kim, H.A., et al., "Shape memory alloy-piezoelectric active structures for reversible actuation of bistable composites" *AIAA Journal*, 48(6): p. 1265-1268, (2010).

List of figures Figure 1: The structural requirements for lightweight shape adaptation	2
Figure 2: The interaction between an adaptive structure, its external loading and actuation for a generic morphing system.	
Figure 3: Forces on airfoil and on the bistable plate	3
Figure 4: NACA 2412 Cp distribution	5
Figure 6: Beam moment diagram with simple supports (left) and with lever (right).	6
Figure 7: Bending moment for standard configuration (without lever) and for lever configuration	7
Figure 8: Bistable panel boundary conditions.	8
Figure 9: Bistable panel model and the two stable state shapes	8
Figure 10: S (septum position) and L (load position)	9
Figure 11: Displacements (a) and deformations (b) with different septum positions	10
Figure 12: Curing profiles and stable states.	10
Figure 13: Snap-through force evaluation test setup	12
Figure 14: Activation forces with variable position of load (L) and septum (S).	12
Figure 17: Bistable flap: the rear spar is the clamp for the short edge of the bistable plate, L profiles are riveted on the same one to create the intermediate septum and two cylindrical ducts allow the air force the laminate. A foam material is introduced between the bistable plate (grey line) and the external skin	
Figure 18: Activation forces vs external ones on the airfoil.	16
List of tables Table 1: Simulated and measured cambers.	11
Table 2: Activation forces for each boundary condition.	9
Table 3: Deformations and displacement for each boundary condition	9
Table 4: Maximum camber	11
Table 5: Experimental/numerical correlation	14
Table 6: NACA 2/12 characteristics Frort Rookmark not define	nad

Table 7: Flap activation forces	1.0
Table 7. Flan activation forces	ır